Journal of Hydrology 630 (2024) 130688

Contents lists available at ScienceDirect

Journal of Hydrology

journal homepage: www.elsevier.com/locate/jhydrol

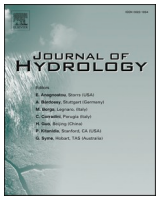

Research papers

# Impacts of climate change on flood volumes over North American catchments

Alexandre Ionno [a,*], Richard Arsenault [a], Magali Troin [a,b], Jean-Luc Martel [a], François Brissette [a]

[a] Hydrology, Climate and Climate Change Laboratory, École de technologie supérieure, Université du Québec, 1100 Notre-Dame Street West, Montreal, Quebec H3C 1K3, Canada

[b] HydroClimat TVT, Maison du Numérique et de l'Innovation, place Georges Pompidou, 83 000 Toulon, France

ARTICLE INFO

This manuscript was handled by Marco Borga, Editor-in-Chief, with the assistance of Christian Massari, Associate Editor.

*Keywords:*
Flood volume
Climate change
Hydroclimatology
Uncertainty analysis
Hydrological modelling

ABSTRACT

Climate change is expected to increase the frequency and intensity of extreme events, such as droughts and floods. Assessing the impacts of climate change on flood volumes is crucial to provide better management of flooding disasters given the devastating consequences they can cause. Using flood volume instead of flood peak is critical because the latter focuses on the highest possible discharge observed during a flood event, while flood volume also considers flow duration, which is an important factor in terms of the hazard caused to the surrounding environment. This study aims to evaluate the overall impact of climate change on floods caused by long-duration flows exceeding synthetic flooding thresholds. These flows are used to compute flood storage with various flow thresholds increasing from the 50th to 95th percentile of annual maximum observed discharge over a large sample of 1403 North American catchments. This study also aims to evaluate the contribution of each uncertainty source of the ensemble approach (climate models, bias-correction methods, and hydrological models) on future flood volumes. The results show that flood volumes are expected to decrease in western mountainous areas, the Great Lakes region, and the Maritimes, while increases are expected over most of eastern North America. The study finds that climate models contribute the most to the variance of flood volume uncertainty, followed by hydrological models. Overall, this study provides projected flood volume changes for North American catchments from a comprehensive ensemble that includes eleven climate models driven by two RCP scenarios and four hydrological models of varying complexity. This leads to a large-sample assessment of future flood volumes that could be useful to policymakers for making better-informed decisions in flood risk management.

## 1. Introduction

Climate change is expected to increase the frequency and intensity of extreme events, such as droughts, floods and precipitation events (Aldous et al., 2011; Arnell & Gosling, 2013; Martel et al., 2022), primarily due to anthropogenic impact (Masson-Delmotte et al., 2021). Anthropogenic climate change is causing more intense precipitation events, which increase the likelihood of floods (Guhathakurta et al., 2011; Tabari, 2020). In particular, spring floods in northern regions are likely to occur earlier by up to one month due to earlier snowmelt (Döll & Zhang, 2010; Arnell & Gosling, 2013). Climate change factors such as variations in extreme temperature or heavy precipitation events also increase the likelihood of floods, with potential impacts on dam safety, altering rivers' hydrology and water quality, and affecting surrounding populations (van Vliet et al., 2013; Fluixá-Sanmartín et al., 2018).

Land use and land cover also have an impact on the hydrological regime (Murdoch et al., 2000; Miller et al., 2002; Carvalho-Santos et al., 2016; Rasouli et al., 2019; Zhou et al., 2019). The removal of forests and shrubland increases surface runoff (Dadhwal et al., 2010; Koneti et al., 2018), while urbanization decreases infiltration rate and, by extension, increases water stress (Rasouli et al., 2019). Similarly, regions with a high percentage of agricultural practice can lead to increased surface runoff and increased water demand, affecting the overall water availability (Miller et al., 2002; Aldous et al., 2011; Carvalho-Santos et al., 2016).

Many climate change impact studies on hydrology have been conducted using models to translate projected climate changes into hydrological responses (Döll & Zhang, 2010; Guhathakurta et al., 2011;

* Corresponding author.
*E-mail address:* alexandre.ionno.1@ens.etsmtl.ca (A. Ionno).

https://doi.org/10.1016/j.jhydrol.2024.130688
Received 25 January 2023; Received in revised form 29 November 2023; Accepted 26 December 2023
Available online 23 January 2024

Troin et al., 2015; Mittal et al., 2016). Different models and combinations of hydroclimatic variables have been applied depending on the objectives of the study (Wilby & Harris, 2006; Döll & Zhang, 2010; Schnorbus et al., 2014; Troin et al., 2018). Some studies have evaluated the impacts of climate change on the occurrence and intensity of extreme climate events, such as floods and droughts (Muzik, 2002; Prudhomme et al., 2003; Aldous et al., 2011; Devkota & Gyawali, 2015; Zhou et al., 2019), while others have focused on the analysis of peak flows in terms of timing, magnitude, volume, flood duration, and intensity (Doll et al., 2009; Veijalainen et al., 2010; Arnell & Gosling, 2013; van Vliet et al., 2013; Devkota & Gyawali, 2015; Mohammed et al., 2015; Zhou et al., 2019; Sun et al., 2021). Obeysekera et al. (2011) point out an expected overall increase in precipitation during the wet season. Most of the aforementioned studies were performed on either a regional or national scale. Few studies have evaluated flood volumes on a continental scale to date (Dankers & Feyen, 2008; He et al., 2022; Ho et al., 2022) including at the macroeconomics level (Koks et al., 2019). This information at this resolution is relevant as it could aid in guiding decision-makers in the design of dams to mitigate future hydrological disasters. Quantifying future flood volumes as well as their potential increases is therefore essential for a comprehensive assessment of flood risk.

The primary objective of this study is to evaluate the impacts of climate change on projected flood volumes in a large sample of catchments in North America over a 30-year window for the reference (1971 to 2000) and future (2070 to 2099) periods. This is important because flood peaks focus solely on the highest discharge of an event, while flood volumes refer to the entire duration of an event, measuring its overall hazard and ability to damage surrounding buildings, ecosystems, and livelihoods. In this context, flood volume is defined as the total volume of water in excess of a given flood-inducing discharge threshold from a single flood event. This study also aims to evaluate the contribution of the main elements of the ensemble approach on the total uncertainty in flood volume projections. Since it remains a major challenge to quantify and reduce individual uncertainties in this approach, this knowledge can provide additional insight into the reliability of the ensemble members for assessing the impacts of climate change on flood volumes. Section 2 presents the study area and associated datasets, and Section 3 describes the method used for generating maximum flood volumes. Section 4 presents the relevant results of the evaluation of flood volumes, while Section 5 provides an analysis of the results. Section 6 provides concluding remarks.

## 2. Study area and data

The main data source for this study was the NAC$^2$H dataset, which contains reference and simulated data for 3540 catchments in North America; 698 catchments are located in Canada and 2842 catchments in the United States. For a more complete description of the scenarios and projections composing the NAC$^2$H database, readers are referred to Arsenault et al. (2020).

To ensure high quality and robustness of the data before starting calculations for flood volume modelling purposes, the following three criteria were used to select catchments from the NAC$^2$H database:

1) catchments required a minimum of 30 years of observed streamflow data in the entire dataset (which covers 1950-01-01 to 2018-12-31),

2) catchments required at least 20 years of observed streamflow data in the reference period, and

3) a maximum of 10 % of missing streamflow data for any of the years over the reference period was allowed.

A 30-year reference period was used to properly estimate the distribution of maximum flows and to minimize the impact of natural variability on smaller windows. This was to better estimate the magnitude of flood-inducing discharge thresholds. Catchments that met these requirements were used for further analysis. In total, 1403 catchments were selected for this study. The catchments' surface areas vary between 300 km$^2$ and 179,000 km$^2$ as shown in Fig. 1. Note that for clarity, catchments with a drainage area larger than 30,000 km$^2$ are nested underneath smaller ones and are not always directly visible.

From the NAC$^2$H database, a subset of the selected ensemble was created by excluding certain elements (Krysanova et al., 2018). The dataset used in this study contains observed hydrometeorological data for the 1403 catchments, as well as bias-corrected climate simulations from eleven climate models of the CMIP5 experiment according to the RCP4.5 and RCP8.5 scenarios (Taylor et al., 2012). NAC$^2$H also provides hydrological model simulations for four hydrological models calibrated with the Kling-Gupta Efficiency metric (KGE; Gupta et al., 2009): GR4J (Perrin et al., 2003; Valéry et al., 2014), HMETS (Martel et al., 2017), HSAMI (Fortin, 2000), and MOHYSE (Fortin and Turcotte, 2007). Ten parameter sets for each model are available within NAC$^2$H, however in this study, only the parameter set with the best calibration was kept. This was done to eliminate the impact of equifinality, which is generally considered to be negligible in terms of its contribution to the overall uncertainty and would add a supplementary dimension to the analyses for little gain (Poulin et al., 2011; Arsenault & Brissette, 2014; Giuntoli et al., 2018; Wang et al., 2020). Additionally, Giuntoli et al. (2018) demonstrate that global hydrological models provide most of the uncertainty, rivalled only by the uncertainty from the climate models for some regions. Considering that, uncertainty associated with the objective function as well as with the parameter set are excluded from the analysis. Moreover, few studies evaluated the uncertainty of components of the hydroclimatic modelling chain on large samples of catchments, and none at date (to our knowledge) evaluate that uncertainty on flood volumes.

The climate model simulations were bias-corrected with four methods of varying complexity, the Daily Bias Correction (DBC; Chen et al., 2013), Multivariate Bias Correction (MBCn; Cannon, 2018), Quantile Delta Mapping (QDM; Cannon et al., 2015), and Two-Stage Quantile Mapping (TSQM; Guo et al., 2019) methods. The reference period used for bias-correction is the 1971–2000 period in NAC$^2$H, while the future period considered is 2070–2099. This leads to a large ensemble of possible future hydrological scenarios.

Additionally, as recommended in other studies, an ensemble of at least ten climate models and multiple downscaling methods is typically sufficient for capturing most of the uncertainty related to the individual ensemble members (Hawkins & Sutton, 2009; Sunyer et al., 2015; Chen et al., 2016; Wang et al., 2020), which was respected in this study. Thus, the ensemble size of climate models in this study (i.e., eleven models) cover adequately the model contribution to the overall uncertainty on flood volume changes due to climate change.

The refinement of the NAC$^2$H was necessary because this comprehensive database includes a very large amount of hydroclimatic simulations. Users of the database are encouraged to generate their own credibility subset of the model ensemble by the NAC$^2$H creators since the database was generated "as-is" without filtering of spurious simulations (Arsenault et al., 2020). Therefore, in this study, all data were taken from a public, pre-computed database such that results are reproducible by any interested party. Users wishing to use the data from the pre-computed database should be aware that all data were calibrated using the same number of years that there are on the separate periods. As it has been shown previously, calibrating on all available data provides more robust hydrological simulations than using a split sample calibration–validation approach (Arsenault et al., 2018). Nonetheless, an evaluation of calibration period simulations was performed to assess the quality of the calibration according to four metrics, as shown in Fig. 2: Kling-Gupta Efficiency (KGE; Fig. 2a), Percent bias (Fig. 2b), Coefficient of determination (Fig. 2c) and mean-normalized Root Mean Square Error (NRSME; Fig. 2d). Table 1 provides the elements defining the selected subset in this study.

In general, the models present satisfactory metrics between the observed and simulated streamflow, as seen in Fig. 2. While some

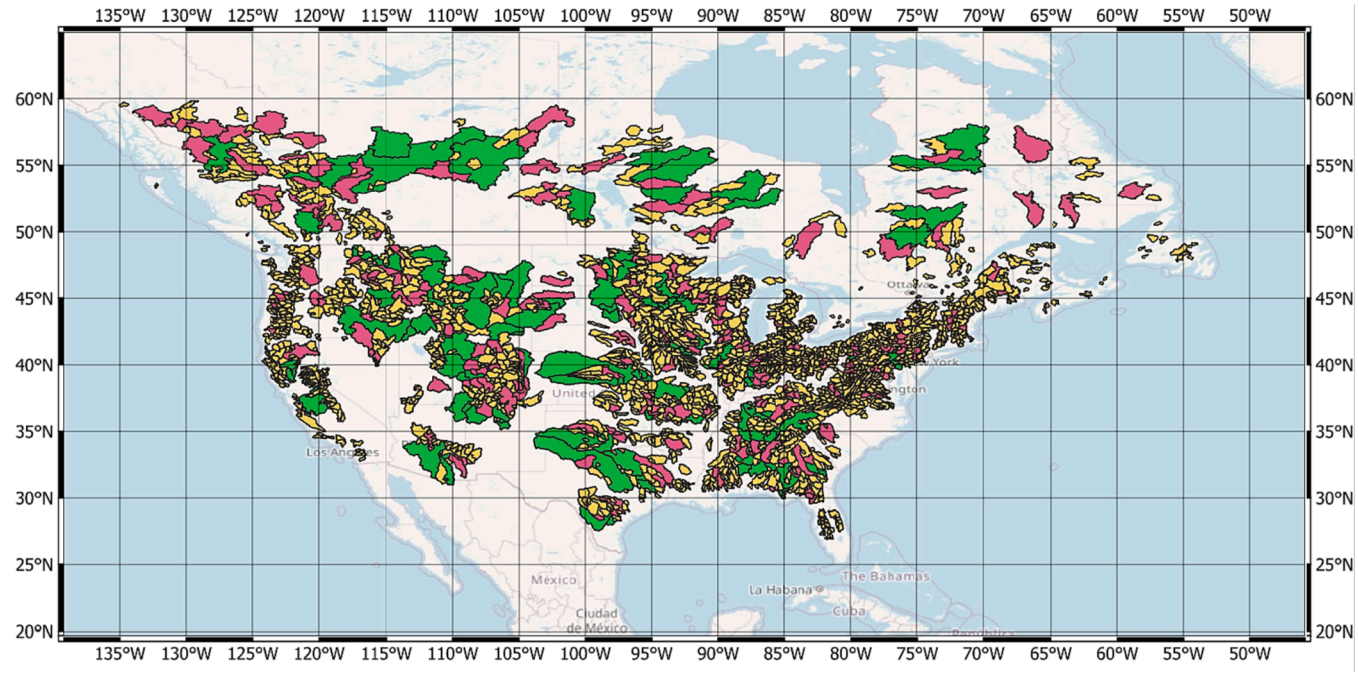


**Fig. 1.** Location of the 1403 catchments in this study, covering Canada and the United-States The larger catchments (>30,000 km$^2$) are colored in green, medium catchments (10,000–30,000 km$^2$) in pink, and the smaller ones (<10,000 km$^2$) in yellow to better distinguish nested catchments. (For interpretation of the references to colour in this figure legend, the reader is referred to the web version of this article.)

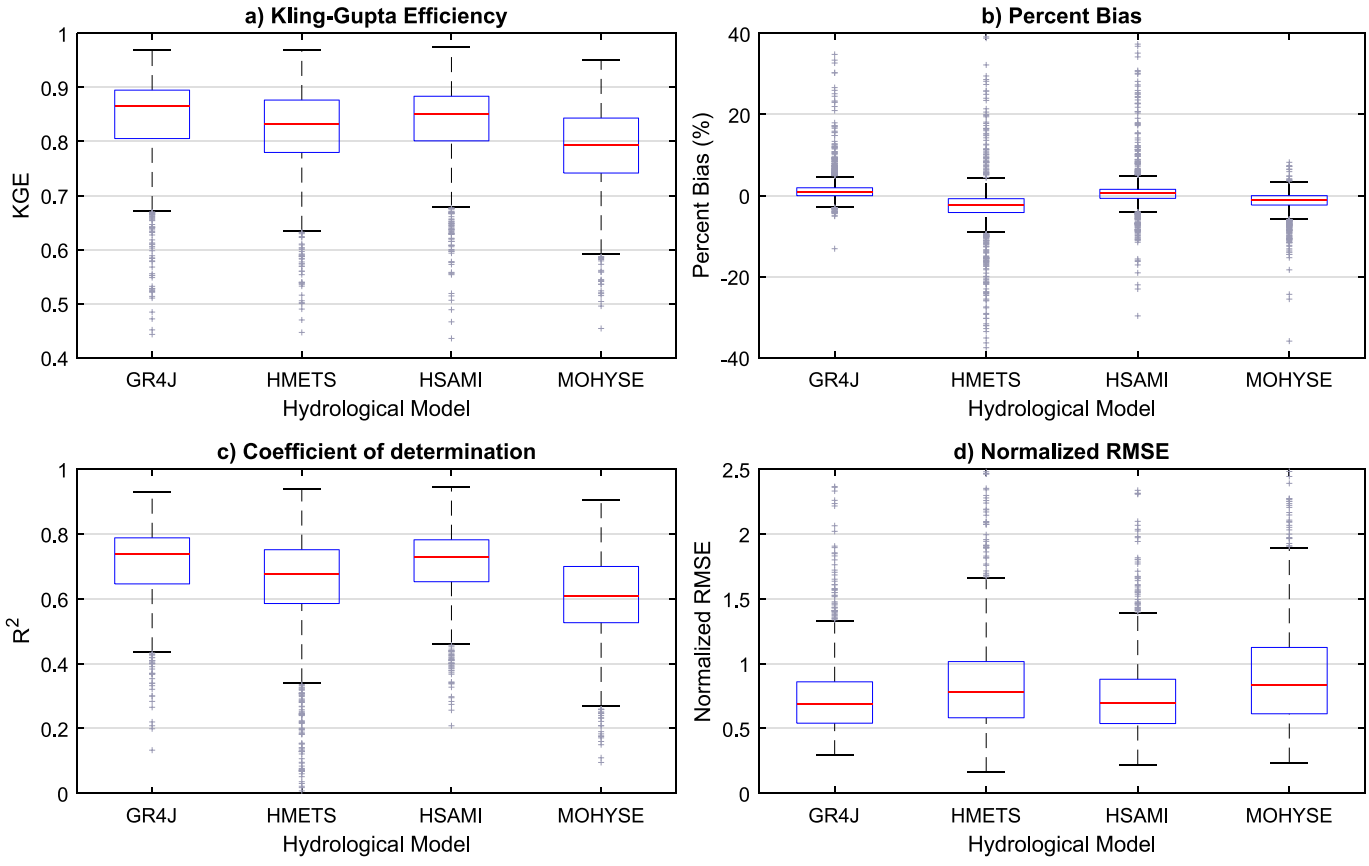


**Fig. 2.** Evaluation of streamflow simulations over the calibration period for the 1403 basins simulated by the four hydrological models. Metrics are (a) the Kling Gupta Efficiency, (b) the Percent bias, (c) the Coefficient of determination, and (d) the mean-normalized Root Mean Square Error. Each boxplot quantifies the difference between the observed and simulated streamflow over the calibration period. Grey markers indicate outliers, while the red horizontal line identifies the median value. The blue box represents the interquartile range (25th – 75th percentiles) and the whiskers present the last value not identified as an outlier. (For interpretation of the references to colour in this figure legend, the reader is referred to the web version of this article.)

**Table 1**
Elements composing the selected ensemble after filtering of the NAC$^2$H database.

| | | |
|---|---|---|
| **Climate models** | ACCESS1-0 | ACCESS1-3 |
| | CanESM2 | CSIRO-Mk3-6-0 |
| | FGOALS-g2 | GFDL-ESM 2G |
| | GFDL-ESM 2M | GISS-E2-R |
| | MIROC5 | MIROC-ESM |
| | MIROC-ESM-CHEM | |
| **RCP scenarios** | RCP4.5 | RCP8.5 |
| **Bias correction methods** | DBC | MBCn |
| | QDM | TSQM |
| **Hydrological models** | GR4J | HMETS |
| | HSAMI | MOHYSE |
| **Calibration parameter sets** | 1 | |
| **Objective function** | KGE | |
| **Number of catchments** | 1403 | |

outliers are present for each metric and for each model, an analysis shows that the outliers represent different watersheds for each model, hinting that some models are more appropriate than others for certain catchments. Nonetheless, all models show strengths in various circumstances and provide useful information for the remainder of this study.

## 3. Methodology

### 3.1. Evaluating maximum flood volumes

The steps for generating extreme flood volume projections are detailed below. This study evaluates the impacts of climate change on both peak flows ($m^3.s^{-1}$) and the flood event duration (s) such that floods should be considered in terms of flood volumes ($m^3.s^{-1}.s = m^3$). To visualize these volumes, they are represented by the amount of water that would need to be stored in a hypothetical reservoir to prevent flows from exceeding a specific threshold for each catchment. To simplify calculations and avoid overgeneralization of the regional natural variability, the reservoir does not consider any factors such as evapotranspiration or infiltration rate. For example, Fig. 3 shows a hydrograph with a flood-inducing discharge threshold value of 1130 $m^3.s^{-1}$. The threshold was obtained by calculating the 50th percentile of the distribution representing the maximum annual observed streamflow. All water above this threshold is considered floodwater (shaded area in Fig. 3-a) and stored in the hypothetical reservoir until flows fall below the threshold (Fig. 3-b), at which point the water is released back into the river. The flood volume for this event would be the maximum cumulative storage attained during this process. In this example, the maximum flood volume is 2,9E + 8 $m^3$ for the period between late April to June.

To estimate the thresholds, the maximum annual flow values over the observational period (1950 to 2010) were calculated. Followed by the calculation of the selected thresholds (i.e., 50th, 75th, 90th, and 95th percentiles) from the empirical distribution of observed maximum annual discharge values). These values provide a constant baseline for what constitutes a flood event for a given catchment; they do not reflect the actual varying flood-inducing discharge threshold values of different rivers and locations. They are indicative of future change, and not of absolute fluvial flooding risk in these rivers. However, the aim of this study is to evaluate projected changes in flood volume, and a threshold was required to define the point at which a river is in a flooding state. Hence, maximum annual flow values serve as approximations of thresholds that can reasonably be considered as a flood-inducing discharge threshold. Although the flood estimations are based on empirical distributions (rather than fitted distributions) for simplicity's sake, this does not influence the estimation of the climate change impact on flood volumes. Indeed, the potential impacts of projected climate change on flood volumes are inferred by evaluating the relative difference between the future and reference period flood volumes using these thresholds as flood-generating flows. However, this study does not analyze the impacts of climate change on the percentiles of floods.

The maximum flood volume was calculated using a simulator that tracks the hypothetical reservoir storage, inflows, and outflows based on the flood-inducing discharge threshold and simulated flows on a day-to-day basis (Fig. 4). For every daily time step in both 30-year windows (the reference and the future periods), the difference between the simulated daily flowrate and the selected threshold flowrate is calculated. If the daily volume exceeds the threshold, the excess water is stored in the reservoir. Otherwise, the storage volume remains at zero or, if the reservoir is storing water, it releases flows at a rate equal to the difference between the threshold and the natural streamflow. The maximum storage value in the 30-year span for each simulation is conserved to consider the worst-case-scenario flood event. This applies to every model run, taking into consideration every possible combination of ensemble members and percentiles for a total of 2112 possible combinations per catchment as per Table 1.

### 3.2. Statistical analysis

Maximum flood volumes were normalized by calculating the ratio of volume to the catchment drainage area, resulting in units of mm before a comparison between catchment sizes. This ratio was called the "Flood Depth Equivalent" (FDE) for clarity in this study. Then, statistical tests were conducted to evaluate the relationships between the physical characteristics of the catchment and the median FDE values using the Pearson correlation test. Physical characteristics (latitude, longitude, elevation, drainage area, as well as crop, forest, grass, shrub, snow, urban, water and wetland land cover types) are all taken from the open-access NAC$^2$H database.

Several tests were performed to evaluate the resulting maximum flood volumes. Firstly, the median volumes of the ensemble for the reference and future periods were compared to estimate potential flood volume changes caused by climate change. Because it is not possible to know which member in the ensemble is the most representative of actual future hydrological conditions, the median of the ensemble of maximum volumes was calculated for each catchment from all members in the selected subset. This ensures a robust approximation of the climate model estimates for each catchment and for each period (reference and future). The significance of the results was evaluated with the non-parametric Wilcoxon test applied on the distributions of flood volumes in the reference and future periods for each catchment. Secondly, empirical cumulative distribution functions (CDFs) of maximum flood volumes were generated to evaluate how the ensemble components (e.g., hydrological model (HM), climate model (GCM), bias correction method (BCM), and emission scenarios (RCP)) contribute to the overall uncertainty under both RCP scenarios. To further evaluate model performance, the bias percentage between the observed and simulated maximum flood volumes in the historical period (1971–2000) was calculated using four percentile thresholds. This was done to evaluate how the hydrological models performed in reproducing the observed maximum flood volumes and their underlying hydrographs. Lastly, a n-way ANOVA (analysis of variance) was performed to assess the contribution of each component of the processing chain to the total uncertainty. By using the four elements (GCMs, HMs, BCMs, and RCP), a second-order variance analysis was computed based on the results obtained for each of the four percentile-based threshold values (50th, 75th, 90th, and 95th) in Section 4.1. The analysis was limited to the second-order since almost all the variance could be explained at this stage. For each of the 4 threshold values, 14 sets of orders (4 main effects terms, 6 first order and 4 s order interactions) were evaluated in terms of their contribution to the total variance. This allows to identify which element or set of elements among the HM, GCM, BCM or RCP contributes most to the total uncertainty.

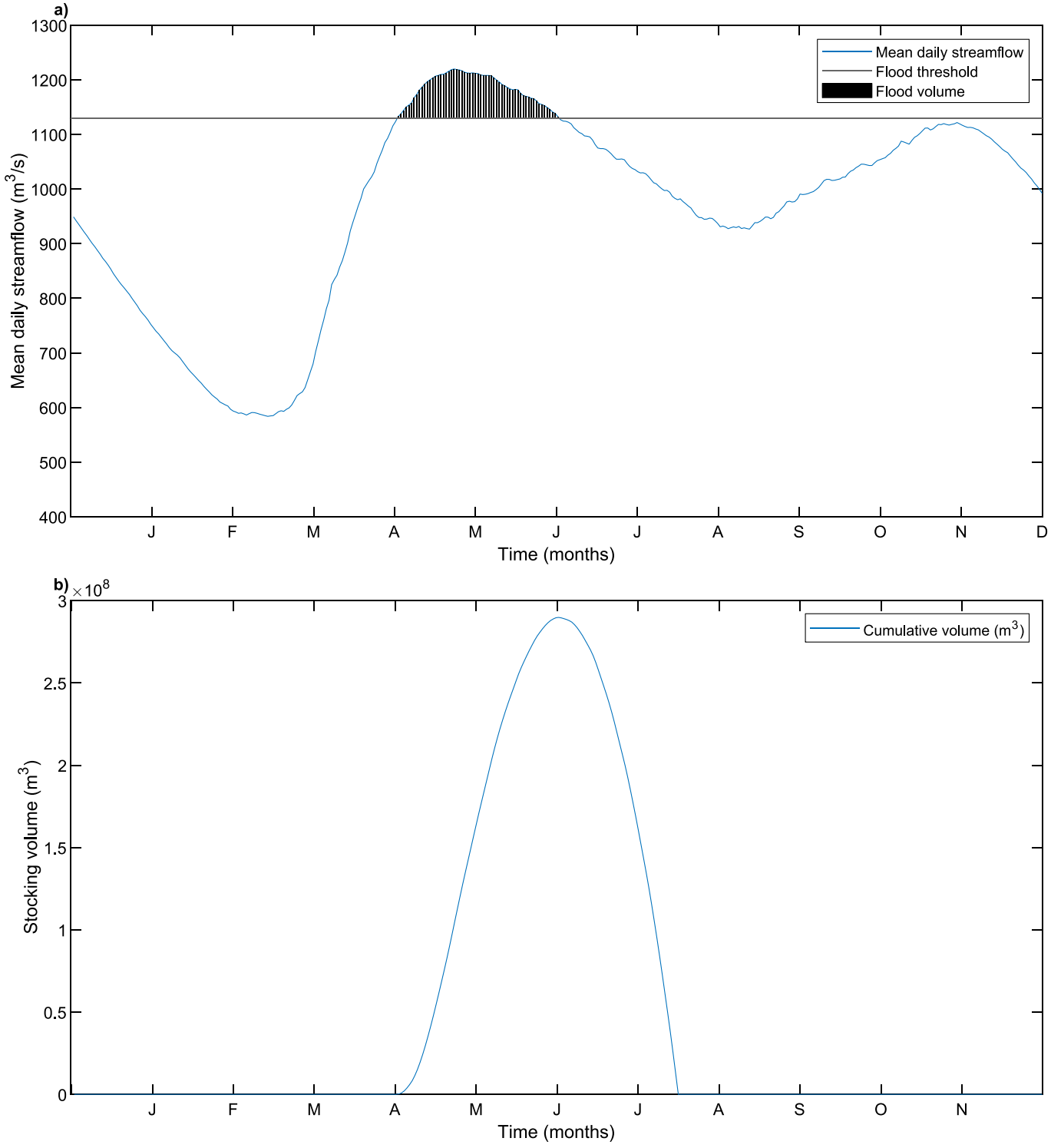


**Fig. 3.** An example of flood volume computation. The shaded area between the hydrograph and the 50th percentile flood-inducing discharge threshold constitutes the flood volume for a given event.

## 4. Results

### 4.1. Maximum flood volumes estimated by the flood volume simulator

Following the results obtained for the flood volumes, Fig. 5 shows the median peak FDE across all ensemble members per catchment for the 50th percentile flood-inducing discharge threshold for the reference period (Fig. 5-a), and the future period under the RCP4.5 (Fig. 5-b) and RCP8.5 (Fig. 5-c) scenarios, as well as the difference between the reference and the projected future peak flood volumes under the RCP4.5 scenario (Fig. 5-d) and the difference between the reference and the projected future peak flood volumes under the RCP8.5 scenario (Fig. 5-e). Further, Figs. S1 to S3 in the supplementary materials depict the results for the remaining percentile thresholds (from the 75th to the 95th percentile) under the future RCP4.5 and RCP8.5 scenarios.

An increase in FDE is observed on the west and southeast coasts of

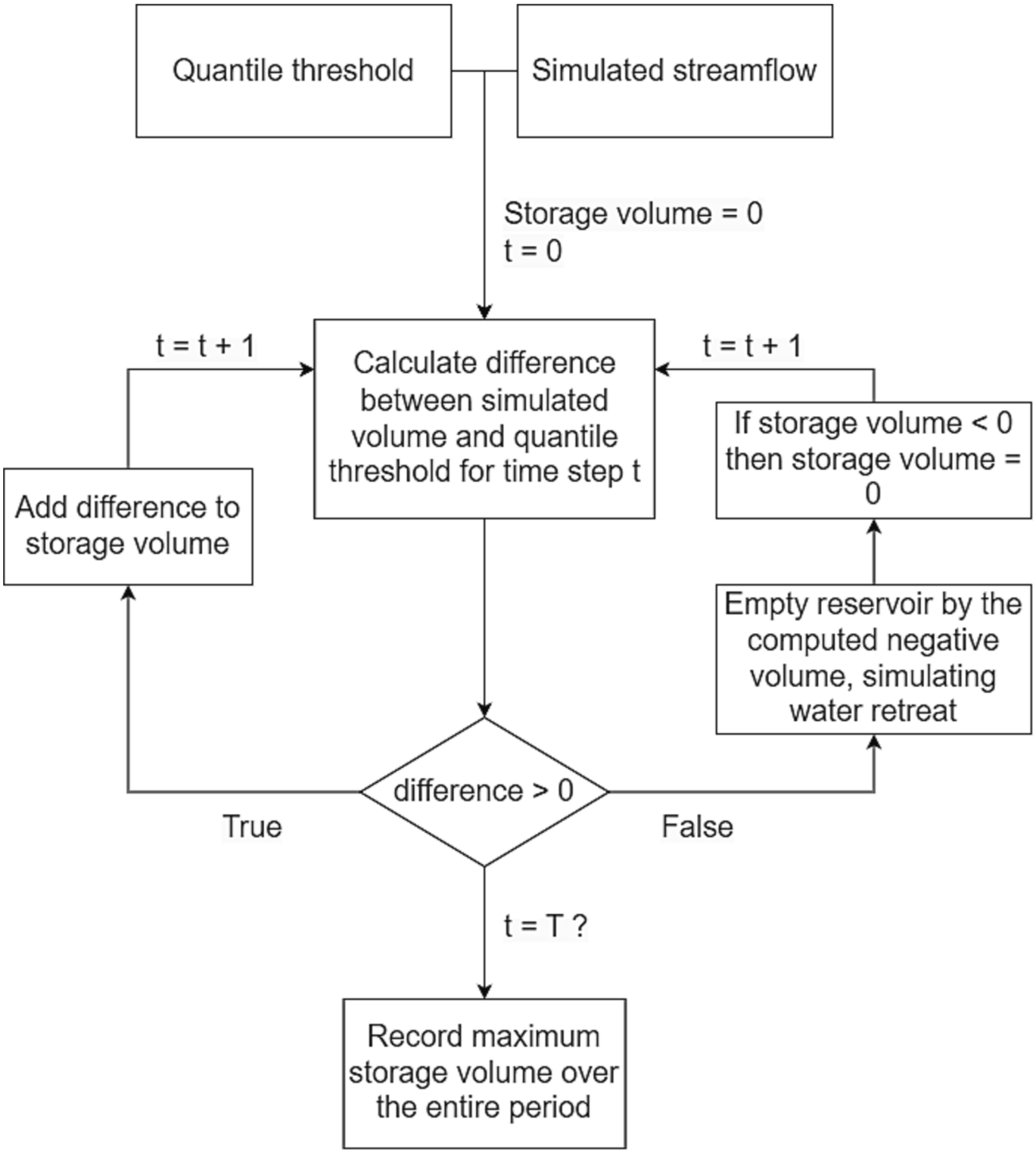


**Fig. 4.** Schematic representation of the daily simulator.

North America, while a decrease in FDE is likely to occur in mountainous areas as well as in regions near the Great Lakes (Fig. 5, panels a-c). Very little changes in FDE are expected for the rest of the study area. Peak flood volumes decrease as the threshold increases from the 50th to 95th quantiles (Table 2), as a higher flow is required to reach the threshold value. Large catchment areas (with a mean drainage area of 14700 km$^2$; Fig. S4b) located in high elevation regions (e.g., between 1500 m and 3500 m; Fig. S4a) display the largest decreases in flood volume. The dominant land cover types for these catchments are forests (Fig. S5b), grasslands (Fig. S5c), shrublands (Fig. S5d), snow (Fig. S5e), and water (Fig. S5g). On the other hand, catchments with a smaller size (mean drainage area of 6400 km$^2$; Fig. S4b) situated in low to medium elevation regions (<1500 m; Fig. S4a) provide the largest increases in flood volumes; croplands (Fig. S5a), urban zones (Fig. S5f), and shrublands (Fig. S5d) are the dominant land cover characteristics of these catchments.

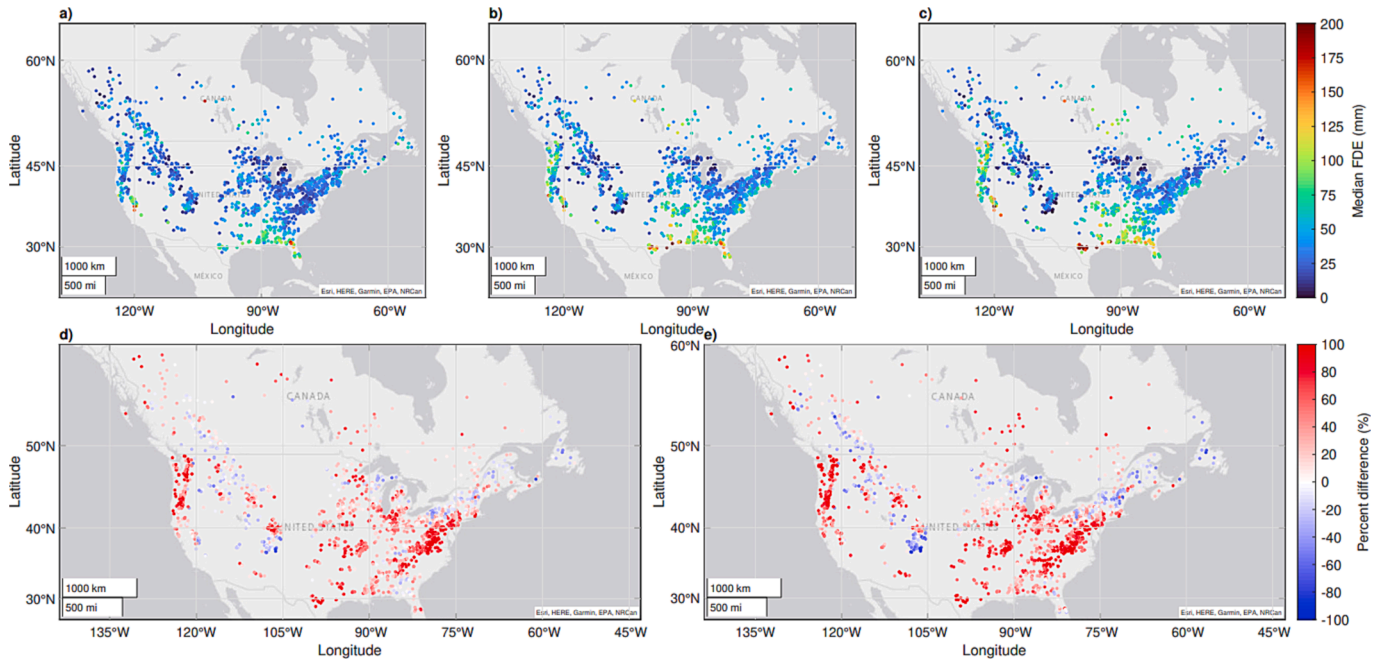


**Fig. 5.** Median normalized peak flood volumes (FDE) per catchment for the 50th percentile for the 1971–2000 reference period (a), the 2070–2099 future period under the RCP4.5 scenario (b), and the RCP8.5 scenario (c). Differences between the projected and the reference maximum flood volumes under the RCP4.5 and RCP8.5 scenarios are presented in panels (d) and (e), respectively.

**Table 2**
Minimum and maximum FDE values over the entire set of catchments for the RCP4.5 and RCP8.5 scenarios, and per threshold value.

| Future emissions scenario | Percentile threshold | Minimum FDE (mm) | Maximum FDE (mm) |
|---|---|---|---|
| RCP4.5 | 50 | 2.5 | 382 |
| | 75 | 0 | 220 |
| | 90 | 0 | 175 |
| | 95 | 0 | 160 |
| RCP8.5 | 50 | 0 | 400 |
| | 75 | 0 | 220 |
| | 90 | 0 | 160 |
| | 95 | 0 | 140 |

Results for the 75th to the 95th percentiles show a decreasing number of catchments with changes in maximum flood volumes in both scenarios (Figs. S1-S3). This is because as the threshold values increase, there is a progressively larger number of catchments that have a reference peak flood volume of 0, making the ratio computation impossible. Indeed, flows in the reference period are based on the observations, but are generated from climate model simulations. Therefore, the flood-inducing discharge thresholds, which are computed based on observations, are not in perfect agreement with the reference period simulations from the climate model even considering bias-correction, since the bias-correction ensures the climate is similar but the natural variability within the model remains. In some cases, the selected threshold value is simply higher than the maximum peak flow of the reference period. In these cases, instead of illustrating the percentage change between the reference and future periods, the results show the absolute change in terms of mm (Fig. 6). Note that Fig. 6 only displays the results for the catchments that had no flood events in the reference period. As such, as the percentile threshold increases, fewer catchments have flood volumes in the reference period leading to more catchments displayed in Fig. 6. Also, as the thresholds increase, the floods are less likely to occur, and those that occur have less flood volume. Further, it is important to note that all catchments for the 50th percentile (Fig. 5) have a peak flood volume for the reference period and are not included in this analysis.

From Fig. 6, the catchments with an increase in peak flood volumes are located on the west coast and eastern side of the United States for the 75th and 90th percentiles (Fig. 6-a, 6-b, 6-c, and 6-d), and in the south of the United States for the 95th percentile (Fig. 6-e and 6-f).

Further, the set of catchments with reference peak flood volumes greater than 0 (Fig. 5) was divided into two categories for each RCP scenario and flood-inducing discharge threshold (Table 3). The categories are (1) catchments with decreasing flood volumes in the future period compared to the reference, and (2) catchments with future increases in flood volumes. It is noteworthy that for both RCP scenarios, the percentage of catchments in each category remains almost constant, with an approximately 20 % – 80 % split, respectively, regardless of the threshold value. This implies that as the thresholds increase and fewer catchments experience floods in the reference period, the remaining catchments react with the same trend, showing the robustness of the results to the selected threshold value. There are slightly fewer catchments with increases in flood volumes for the RCP8.5 scenario compared to the RCP4.5 scenario.

Lastly, Fig. 7 demonstrates catchment location where results are significant (green points) and non-significant (red points) with respect to the emissions scenario and the threshold value. It is observed that regions surrounding the Great Lakes as well as the mountainous region of western North America are typically non-significant. This is also true for a small subset of catchments on the west- and south-east coasts of the United States and central Canada. Further, Table 4 shows significance levels in concordance with the different emission scenarios and thresholds. Significance levels increase as percentile thresholds increase.

### 4.2. *Correlation results between FDE and catchment characteristics*

With regards to the results obtained for the correlation tests (Table 5), no useful correlations were found between median FDE values and individual catchment characteristics. This is because the coefficient of determination ($R^2$) used in the study was below 1 % for all combinations. This means that less than 1 % of the variance could be explained by any single one of these variables.

Note that for more information concerning the catchment

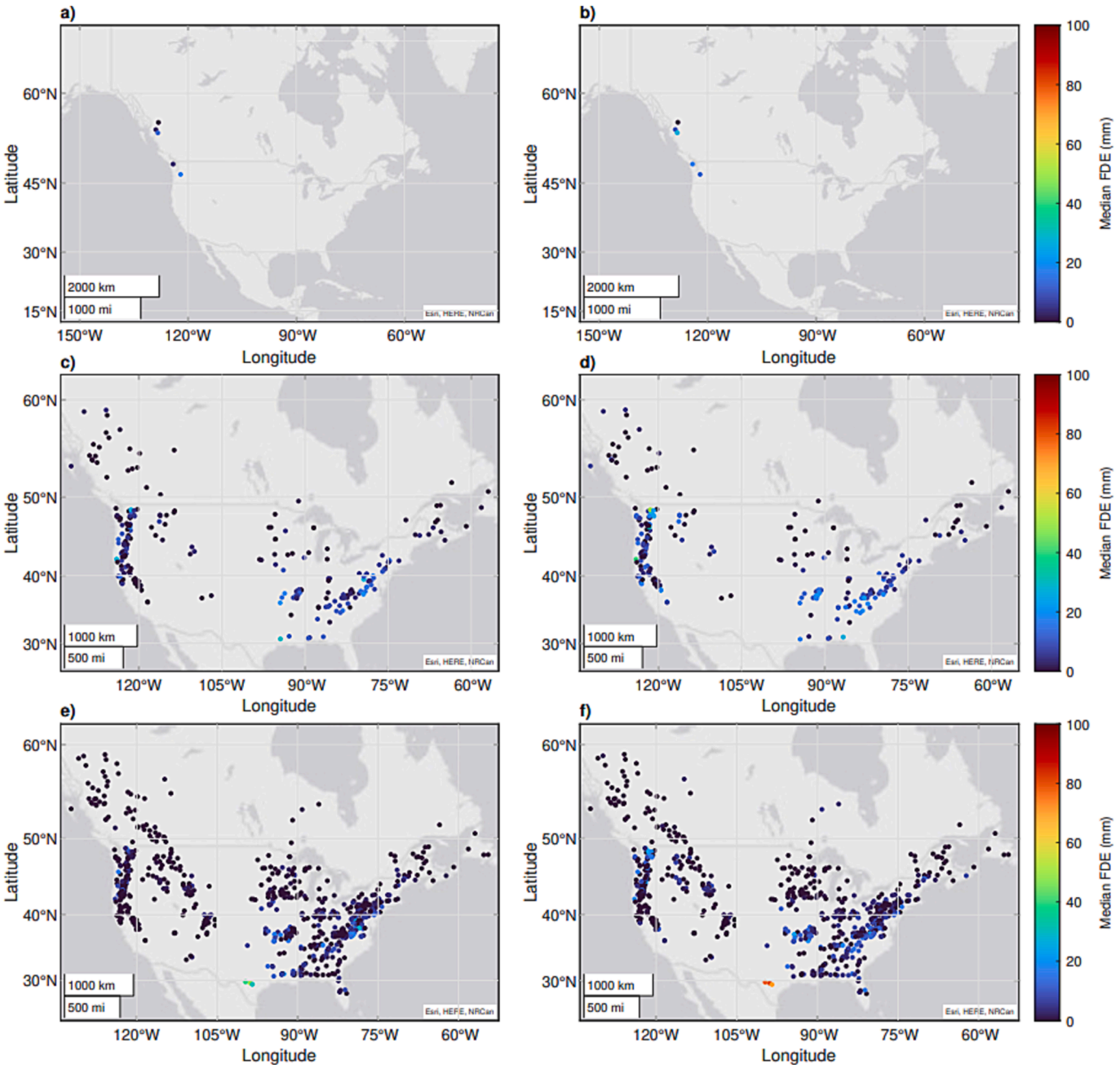


**Fig. 6.** Median normalized FDE for catchments with no reference storage volume for the future period under RCP4.5 (a, c, e) and future period under RCP8.5 (b, d, f); for the 75th (a, b), 90th (c, d), and 95th percentile (e, f).

**Table 3**
Statistics on the changes in flood volumes over the entire set of catchments for the RCP4.5 and RCP8.5 scenarios, and per threshold value.

| Future emissions scenario | Percentile threshold | Total number of catchments with positive flood volumes in the reference period | Overall decrease in flood volume **No. of catchments** | **(%)** | Overall increase in flood volume **No. of catchments** | **(%)** |
|---|---|---|---|---|---|---|
| RCP4.5 | 50 | 1403 | 320 | 22.8 | 1083 | 77.2 |
| | 75 | 1398 | 255 | 18.2 | 1143 | 81.8 |
| | 90 | 1164 | 195 | 16.8 | 969 | 83.2 |
| | 95 | 705 | 141 | 20.0 | 564 | 80.0 |
| RCP8.5 | 50 | 1403 | 343 | 24.4 | 1060 | 75.6 |
| | 75 | 1398 | 281 | 20.1 | 1117 | 79.9 |
| | 90 | 1164 | 203 | 17.4 | 961 | 82.6 |
| | 95 | 705 | 143 | 20.3 | 562 | 79.7 |

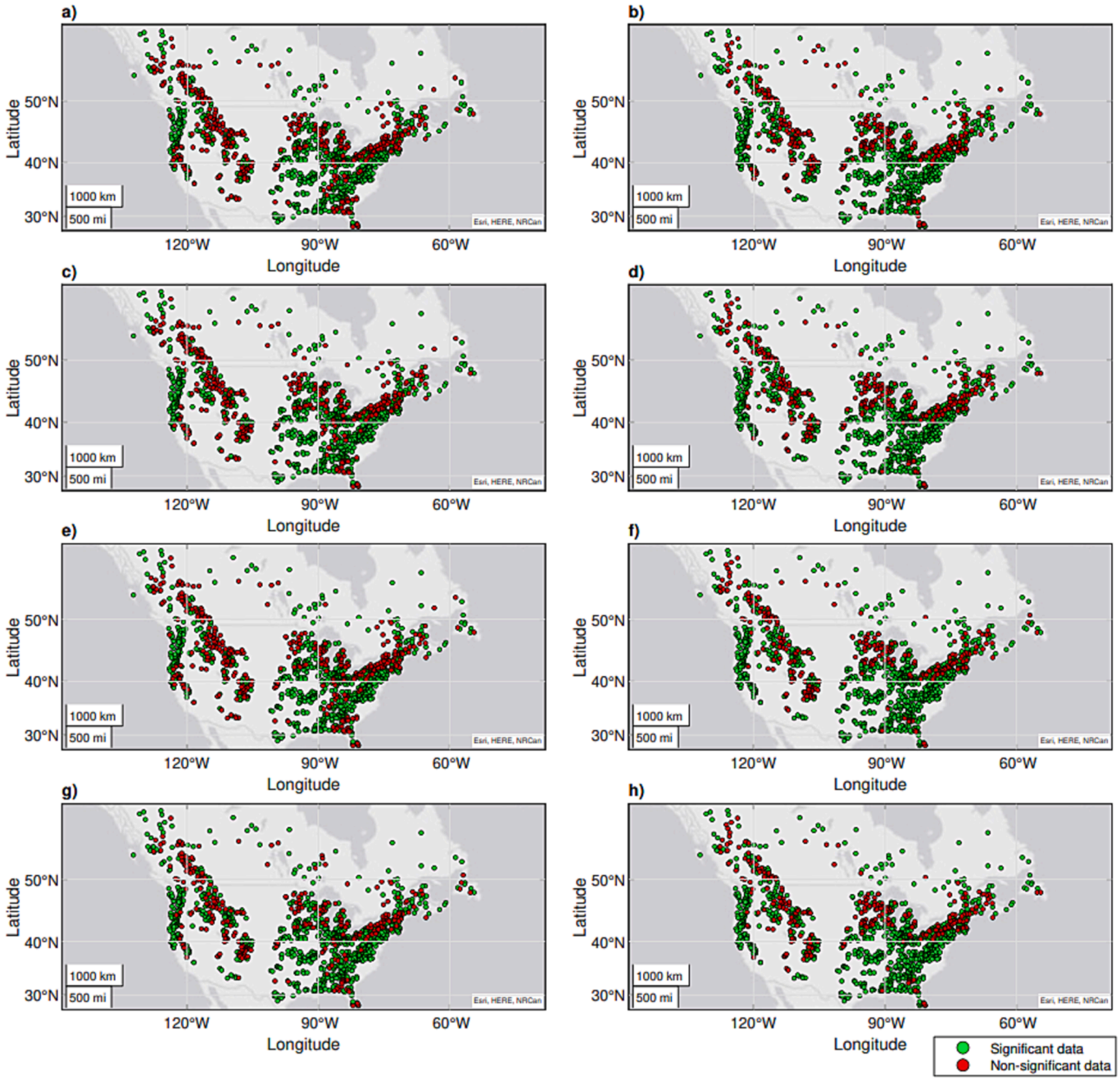


**Fig. 7.** Significance test for catchments with significant results (green circles) and nonsignificant results (red circles) for the RCP4.5 (a, c, d, g) and RCP8.5 (b, d, f, h) scenarios for the 50th (a, b), 75th (c, d), 90th (e, f), and 95th percentile (g, h). (For interpretation of the references to colour in this figure legend, the reader is referred to the web version of this article.)

**Table 4**
Summary of the significance test results over the entire set of catchments for the RCP4.5 and RCP8.5 scenarios, and per flood threshold percentile.

| Future emissions scenario | Threshold Percentile | Catchments with significant results (%) |
|---|---|---|
| RCP4.5 | 50 | 70.9 |
| | 75 | 71.8 |
| | 90 | 75.2 |
| | 95 | 76.7 |
| RCP8.5 | 50 | 78.6 |
| | 75 | 79.1 |
| | 90 | 80.5 |
| | 95 | 82.4 |

characteristics and the method of retrieval, refer to Arsenault et al. (2020). Further, the elevation was calculated as being the mean elevation in relation to mean sea level per catchment, and the land covers represent the permanent land cover for that catchment. For example, snow cover indicates the permanent snow cover that a catchment can have throughout the year.

### 4.3. *Uncertainty of the selected ensemble elements*

The previous results pertain to the median value of the ensemble. Fig. 8 presents the empirical CDFs of the elements composing the full ensemble to assess the variability obtained for the future period under the two RCP scenarios compared to those obtained for the reference period. Note that the distributions in Fig. 8 are truncated to show details

**Table 5**
Correlations between catchment characteristics and median FDE over the entire domain, as well as the associated *p*-value.

| Characteristics | | $R^2$ | *ρ*-value |
|---|---|---|---|
| Latitude (°) | | 0.0023 | 0.0042 |
| Longitude (°) | | 0.0000 | 0.7050 |
| Surface area ($km^2$) | | 0.0028 | 0.0016 |
| Elevation (m) | | 0.0005 | 0.1761 |
| Type of land cover (%) | | | |
| | Cropland | 0.0075 | 0.0000 |
| | Forest | 0.0003 | 0.3002 |
| | Grassland | 0.0003 | 0.3215 |
| | Shrubland | 0.0025 | 0.0029 |
| | Snow | 0.0046 | 0.0001 |
| | Urban | 0.0002 | 0.4619 |
| | Water | 0.0020 | 0.0074 |
| | Wetland | 0.0022 | 0.0053 |

to a better degree where the ensembles diverge the most.

A recurring finding of this analysis is the increase in the projected flood volumes which tend to become more pronounced between the RCP4.5 and RCP8.5 scenarios in comparison to the reference peak flood volumes (Fig. 8). The ensemble spread of the hydrological models contributes to the overall uncertainty in the future flood volume projections (Fig. 8-a), but to a lesser extent than the climate models (Fig. 8-b), which provide the most variability. This could be attributed to the fact that fewer hydrological models make up the ensemble compared to climate models. Lastly, the uncertainty associated with the bias correction methods on the flood volume projections is the least variable overall (Fig. 8-c).

Fig. 9 demonstrates the distribution of simulation flood volume bias calculated for the 50th percentile threshold, with flood volumes computed using the observed flows and the simulated flows on the historical period. This allows evaluating the model error on the historical period, which is likely also present in the reference and future simulations. Each boxplot in Fig. 9 shows the bias between the simulated and observed maximum flood volumes over the entire reference period for all catchments (i.e., each boxplot contains one value per catchment). It can be seen that GR4J and HSAMI provide the most reliable results, while HMETS providing a strong negative bias. The HMETS simulated flows are generally well represented but with a systematic peak flow underestimation, leading to an underestimations of flood volumes compared to a fixed threshold. However, since the results are presented in relative terms (relative change between the reference and future periods), this aspect is not as critical as if the models were used to evaluate absolute flood-based risk.

### 4.4. *Variance analysis of ensemble elements*

This section evaluates the relationships between the ensemble elements and the associated uncertainty within each element in the processing chain. Table 6 presents the results obtained, ordered from the most to least contributing, in terms of maximum contribution from one catchment (column 3), and the average contribution from every catchment (column 4). The first three sets were selected for further analysis as they contributed the most to uncertainty compared to the other eleven sets. Note that the minimum contribution was 0 % in every case scenario.

Results of the uncertainty analysis for the most relevant sets of elements for the four percentile threshold values are presented in Figs. 10 to 12 for sets 1 to 3 (which represent the main effect of HMs and GCMs, and the first order effects of the GCMs and RCPs; see Table 6). Sets 1 (HMs), 2 (GCMs), and 3 (GCMs and RCP) show a decrease in their overall contribution to uncertainty as the percentiles decrease. The individual HM and GCM elements contribute the most to the uncertainty in the projected flood volumes, more than the associated interaction terms. The main BCM effects rank 5th in terms of variance contribution. Set 1 (HM) displays an effect where a decrease in storage volume is observed, while sets 2 (GCM) and 3 (GCMs and RCP) display effect where an increase in storage volume is observed.

Further, sets 1 (GCMs) and 3 (GCMs and RCPs) contribute to the uncertainty over the eastern and western coasts of the United States (Figs. 10 and 11), where the dominant catchment characteristics are cropland, shrubland, urban zones, lower elevations (<1500 m), and smaller drainage areas (approximately 6400 $km^2$ on average). Set 2 (HM) has a localised influence on uncertainty in the mountainous regions of the midwestern United States and Canada (Fig. 12), where the dominant catchment characteristics are forest, grassland, shrubland, snow, water, high elevations (1500 to 3500 m) and large drainage areas (approximately 14700 $km^2$ on average).

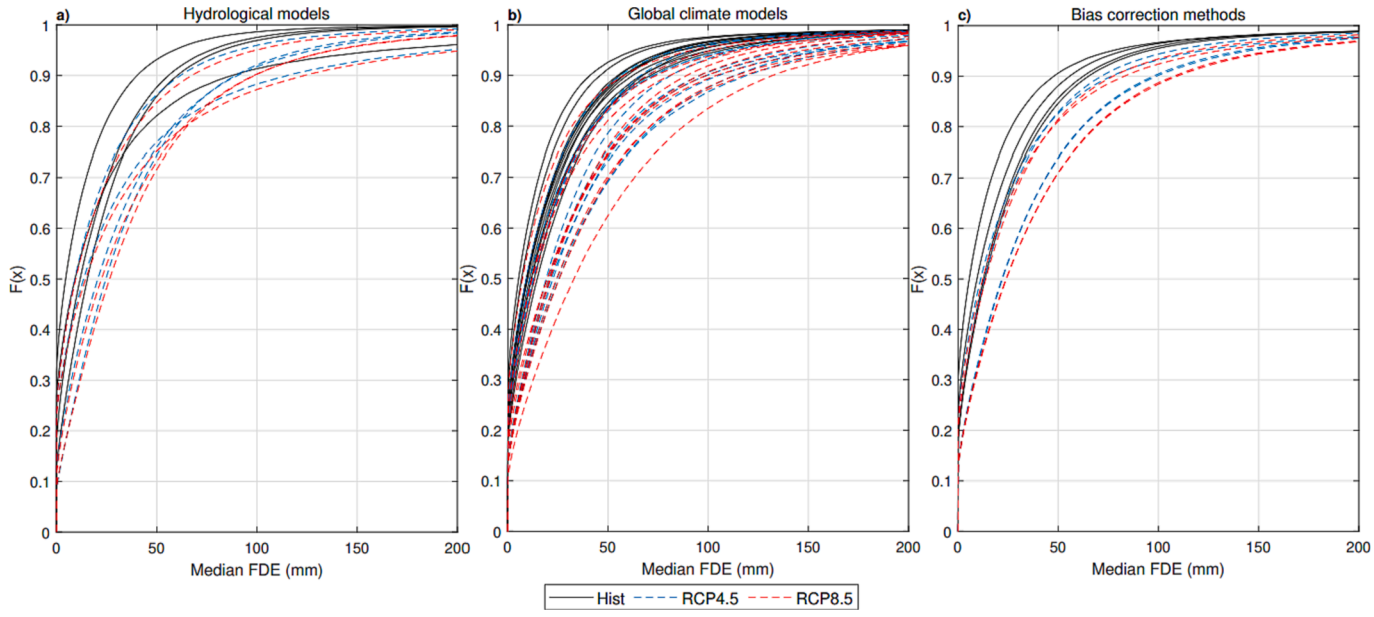


**Fig. 8.** Empirical CDFs under the reference scenario and the future RCP4.5 and RCP8.5 scenarios for the hydrological models (a), the climate models (b), and the bias correction methods (c).

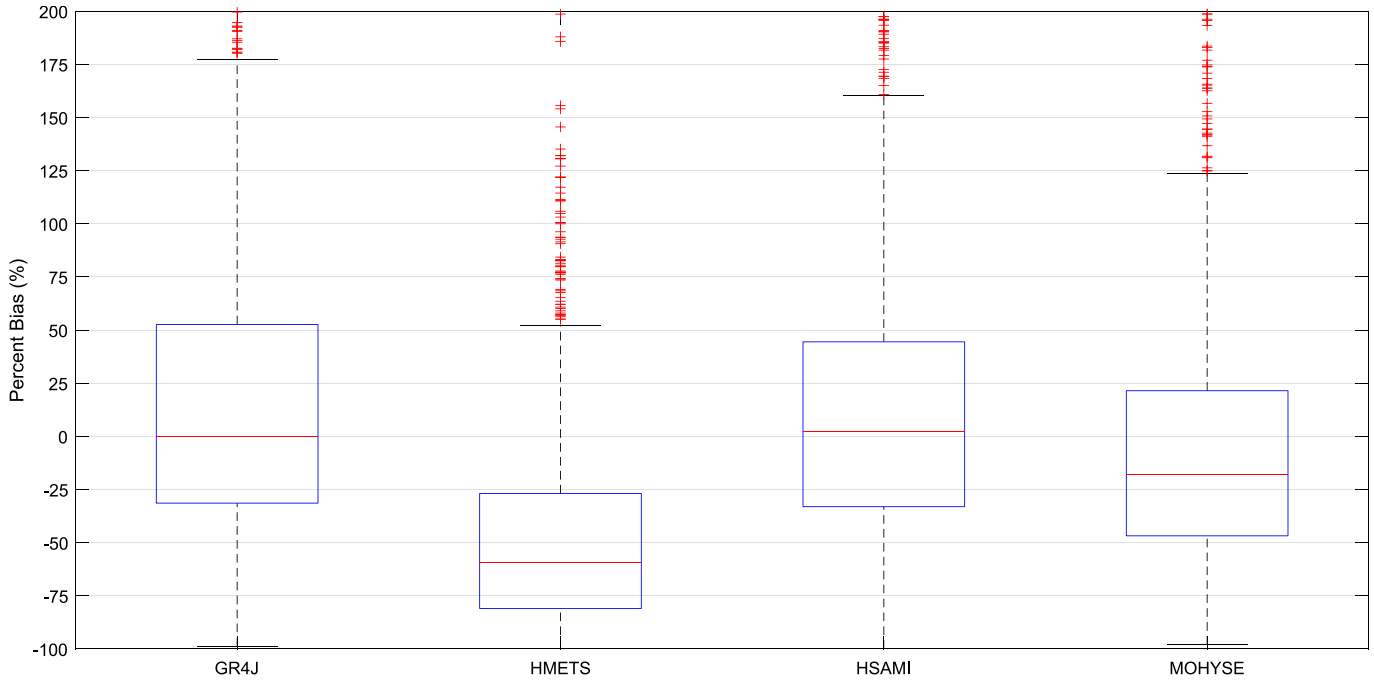


**Fig. 9.** Percent bias between the observed and simulated maximum peak floods on the historical period by catchment and hydrological model for the 50th percentile threshold.

**Table 6**
Ordered contributors to the uncertainty from variance analysis.

| Component set no. | Component set elements | Maximum contribution from one catchment over the study area (%) | Mean contribution from all catchments over the study area (%) |
|---|---|---|---|
| 1 | GCM | 77.3 | 28.1 |
| 2 | HM | 99.8 | 20.9 |
| 3 | GCM and RCP | 56.6 | 15.2 |
| 4 | HM and GCM | 33.2 | 8.5 |
| 5 | GCM and BCM | 49.6 | 7.7 |
| 6 | BCM | 41.7 | 6.2 |
| 7 | HM, GCM and RCP | 32.9 | 6.1 |
| 8 | GCM, BCM and RCP | 31.4 | 5.7 |
| 9 | HM, GCM and BCM | 39.7 | 4.0 |
| 10 | HM and BCM | 35.8 | 1.8 |
| 11 | RCP | 27.2 | 1.7 |
| 12 | HM and RCP | 43.0 | 0.7 |
| 13 | BCM and RCP | 8.5 | 0.7 |
| 14 | HM, BCM and RCP | 25.1 | 0.4 |

HM: Hydrological Model, GCM: Global Climate Model, BCM: Bias Correction Method, RCP: Representative Concentration Pathway.

## 5. Discussion

### 5.1. Projected flood volume changes

From the projections made in this study for the 2070–2099 period, overall increasing flood volumes are expected over a large part of North America, although some areas show decreasing flood volumes. The findings are in agreement with previous studies, which show that river flow discharges (Do, Westra, & Leonard, 2017; Tabari, 2020) and flood volumes (He et al., 2022; Sun, Li, Shan, Xu, & Wang, 2021; Zhou et al., 2019) are projected to decrease in the western regions and increase in the eastern regions of North America.

For catchments that are subject to a future increase in flood volume, the "business-as-usual" scenario (RCP8.5) would lead to the highest increase. This can be explained by the fact that the RCP8.5 scenario projects a higher increase in projected temperature and precipitation compared to the RCP4.5 scenario. Furthermore, as percentile thresholds increase, catchments affected by a change in flood volume maintain a similar geographical distribution, which increases confidence in the results which are geographically robust to the choice of threshold value.

Additionally, maximum flood volumes vary strongly depending on the percentile threshold used. The 50th to 95th percentile threshold analysis displays a decreasing number of catchments requiring larger storage volumes under both scenarios and sensitive to extreme increases; this is in agreement with the study of Prudhomme et al. (2003).

Results obtained for the catchments that experience snowfall and snowmelt seasons show an increase in storage volume needs. However, the literature clearly depicts a decreasing trend of spring flooding amplitude due to climate change, which is contradictory to the present study except in far north catchments (Arsenault et al., 2013; Cochand et al., 2019). Furthermore, as the method used in calculating the daily storage volumes is based on a 30-year window, only the worst-case scenario peak volumes over the 30-year span are retained for each combination. This results in an ensemble of extreme event storage volumes per catchment, although this may be opposite of the observations for mean peak flood volumes in some cases. For example, some northern catchments show increases in flood volumes even though it is expected that snowmelt, the main driving factor of peak flows, should decrease in the future. It is likely that flood volumes are driven by more extreme events under climate change, which likewise impacts the hydrology of these northern catchments.

### 5.2. Uncertainty of ensemble members and land cover types in the projected high flows

Regarding the high number of simulations and element combinations provided in the study, the projected storage volume requirements across North America are robust to the climate model variability and spatial distribution of results. The large number of selected GCMs, HMs, and BCMs results in a large ensemble of possible future hydrological scenarios, capturing most of the uncertainty related to the individual

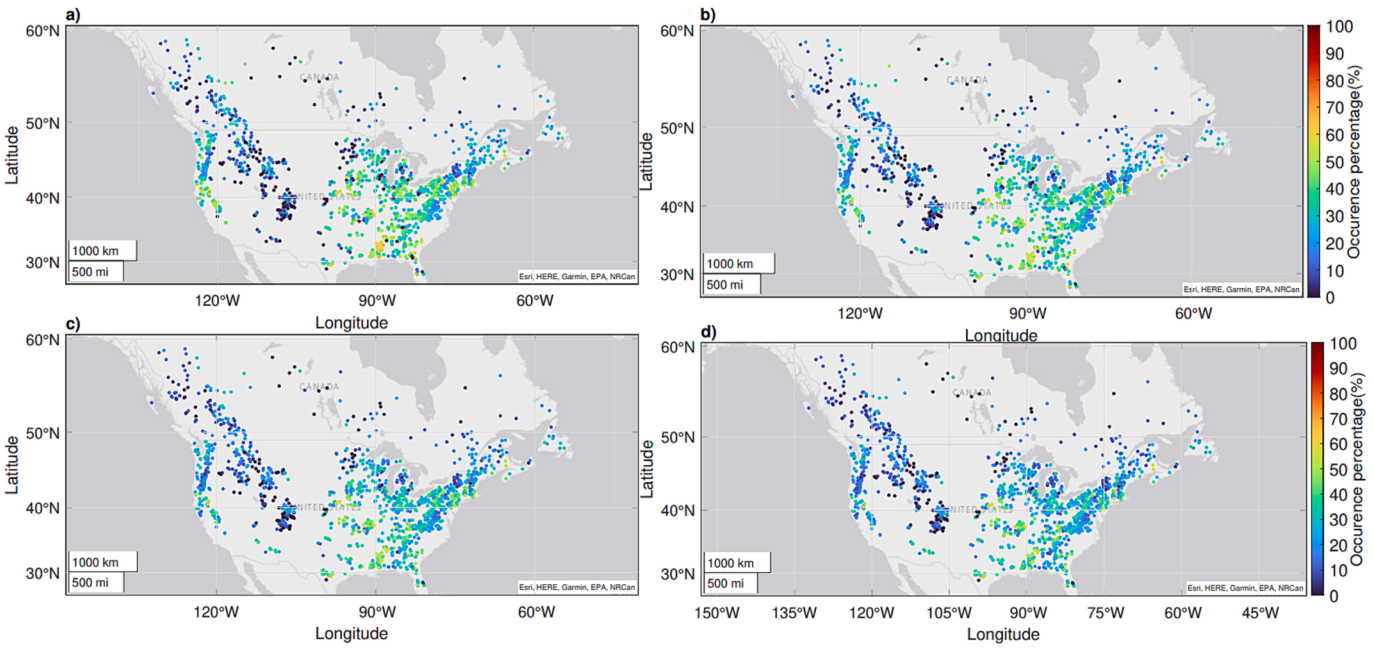


**Fig. 10.** Contribution of uncertainty (%) caused by the GCM element with the 50th percentile (a), the 75th percentile (b), the 90th percentile (c), and the 95th percentile (d).

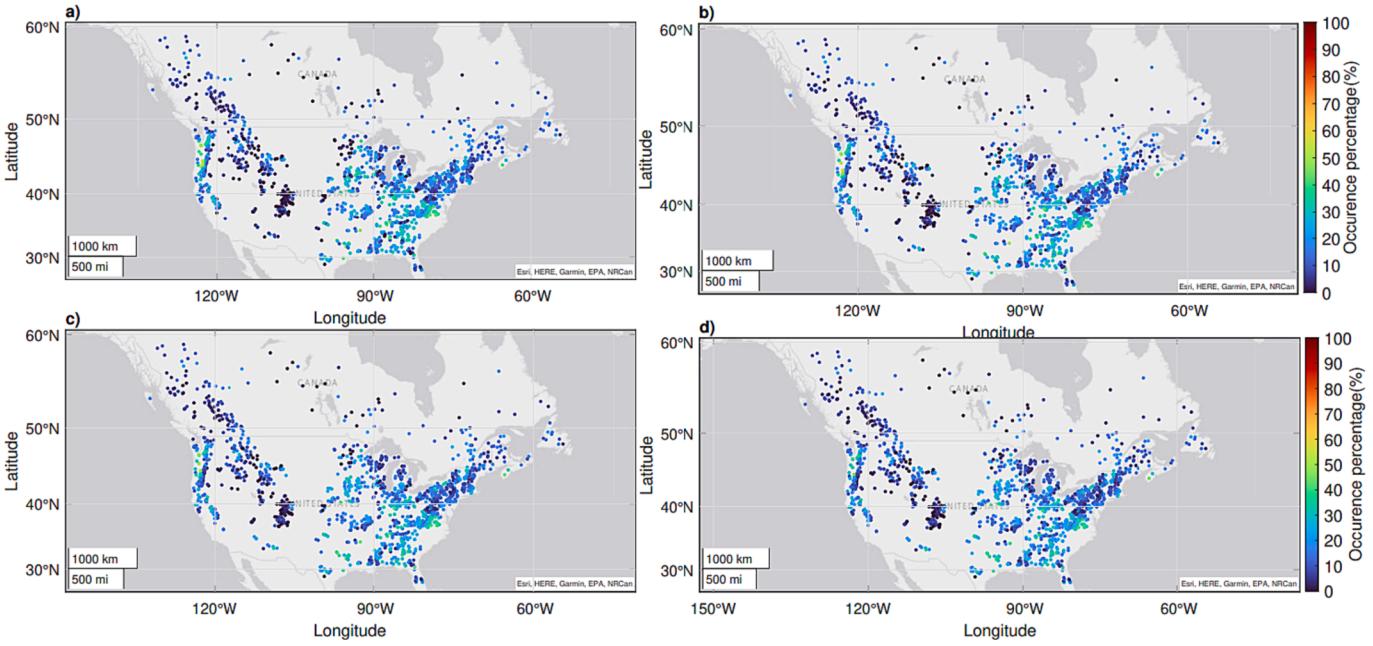


**Fig. 11.** Contribution of uncertainty (%) caused by the GCM and RCP element combination with the 50th percentile (a), the 75th percentile (b), the 90th percentile (c), and the 95th percentile (d).

ensemble members (Miller et al., 2002; Chen et al., 2011; Sunyer et al., 2015; Wang et al., 2020). The use of subsets from the full ensemble to meet the purpose of this study allowed for the generation of a reliable estimate of the ensemble mean.

The top mean contribution to uncertainty for the areas where an increase in the projected flood volumes is provided by the main element GCM, and the first order elements GCMs and BCMs. Oppositely, the mean contribution to uncertainty for the areas with an expected decrease in the projected flood volumes is provided by the main HM element. Overall, the contribution to the total uncertainty from the GCMs is significant for smaller catchments (<6400 $km^2$ on average) of lower elevations (<1500 m) with a small number of different dominant land cover types, while the HMs uncertainty dominates the catchments with a larger surface area (>14700 $km^2$ on average), characterized by a higher elevation (1500 to 3500 m) and a large number of various dominant land cover types. It is important to note that this study did not find any correlation between flood volume changes and catchment characteristics such as land use (Table 5). It is also likely that land use will evolve in the next decades such that the hydrological response might be modified substantially. In this study, catchment characteristics were considered constant, which might also introduce biases between the historical and future period flood volume estimations.

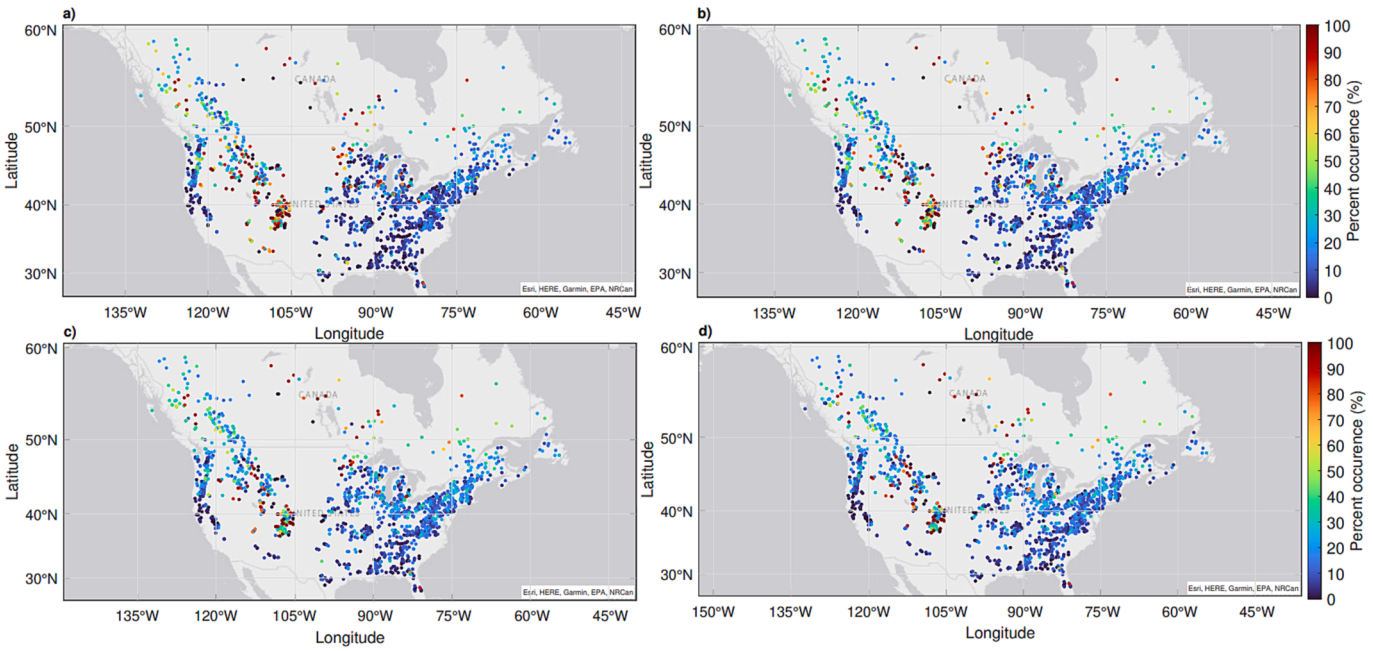


**Fig. 12.** Contribution of uncertainty (%) caused by the HM element with the 50th percentile (a), the 75th percentile (b), the 90th percentile (c), and the 95th percentile (d).

The uncertainty associated with the GCM and HM elements was explored in many studies and has been shown to be the leading contributors in the uncertainty in hydrological modeling (e.g., Knutti et al., 2010; Troin et al., 2015; 2018). In concert with the catchment characteristics, GCMs can also affect the performance of the hydrological model (Karmalkar et al., 2019). Further, the uncertainty associated with the GCMs and BCMs follow close behind the HMs by contributing to high amounts of uncertainty as well; a point studied by other studies (Knutti et al., 2010; Veijalainen et al., 2010; Chen et al., 2011; Poulin et al., 2011; Kim et al., 2016; Troin et al., 2018; Wilby & Harris, 2006). Both elements are known to provide the largest uncertainty on high flows (Gao et al., 2020) and on the projected streamflow values above the 75th percentile (Wang et al., 2020). The GCMs and BCMs uncertainty is substantial for regions with a complex topography (Fluixá-Sanmartín et al., 2018), such as the mountainous areas with large water bodies (i.e., lakes, rivers, wetlands, etc.) and high humidity contents, where the local processes can differ from the GCM representation and BCMs can strongly influence results. Similarly to HMs, it is often the model structure that underrepresents the region's natural variability and fluctuations, thus affecting the model efficiency and performance for climate change impact studies. This could be one of the reasons behind the poor performance of the hydrological HMETS model which provide the least reliable results when comparing percent bias in the historical observation period.

### 5.3. *Limitations and implications for hydrological studies*

The experimental design of this study has some limitations. First, only one objective function was used to evaluate the performance of the hydrological models at simulating high flows. While it is common practice to use the KGE objective function to evaluate the quality of a hydrological simulation in catchments of varying characteristics (Paul & Negahban-Azar, 2018), more objective functions are often required to assess their contributions to the total uncertainty (Poulin et al., 2011; Kouchi et al., 2017; Paul & Negahban-Azar, 2018; Hunter et al., 2021). For example, the Nash-Sutcliffe Efficiency metric (NSE; Nash & Sutcliffe, 1970) is generally used in studies where the high flows are of interest given the quadratic nature of the error function, weighting them more heavily. However, the objective functions and calibration parameter sets are elements that cause very little to no uncertainty in high-flow studies (Wilby & Harris, 2006; Maurer et al., 2010; Chen et al., 2011). The experimental design of this study relies on the NAC$^2$H database, and the only option other than KGE was to select the logKGE metric which is ill-suited for this study.

Even though lumped hydrological models are often used in hydrological climate change impact studies, the inclusion of one or more distributed hydrological models in the ensemble would likely influence the results of streamflow simulations (Maurer et al., 2010). Lumped hydrological models are catchment-scale representations of the transformation of precipitation into discharge and do not provide any spatially hydrological response, compared to distributed hydrological models. In addition, our analysis is based on four quantiles for the calculation of storage volumes; using more quantiles would provide a more comprehensive analysis of the flood volume magnitudes. Additionally, using real flood thresholds as opposed to synthetic ones would be an interesting experiment, as it would allow to explore the response of a particular region's flood to climate change while respecting regional flood protection levels.

Finally, it would be interesting to compare the approach proposed herein to an event-based analysis, where individual flood events could be analyzed both in the historical and future periods. This could be achieved by separating baseflow from event flow and evaluating changes to flood volumes during high-flow events. While perhaps not directly applicable to all catchments (i.e. snowmelt dominated vs rainfall dominated), when it could be applied, this method might provide more accurate results. In this study, we attempted to imitate this concept using the flow quantiles as proxies of baseflow that are constant in time, which is a simplification that could impact the accuracy and reliability of the obtained results.

## 6. Conclusion

The primary aim of this study was to evaluate the potential future evolution of flood volumes over a large sample of North American catchments. Such an evaluation is critical as water storage reservoirs are necessary for sustainable development strategies for many communities. Our evaluations indicate that overall flood volume projections should increase in most areas of North America, with the highest increase in

flood volume projections observed on the west coast of the United States and in eastern North America. However, some regions should experience a decreasing flood volume such as the western Canada, the midwestern United States, and the Great Lakes region in the east of North America. Water retention structures with varying volumes may be necessary to adapt the water storage regarding the flood volume projections. Based on a flood volume simulator that estimates maximum flood volumes based on a flood-level threshold, the mean storage volume required per catchment was calculated for several percentiles based on observed streamflow data.

A decrease in peak flood volumes is expected in high elevation regions (1500 to 3500 m), while an increase in storage volume is expected for low elevation regions (<1500 m). Small catchment areas (areas smaller than 6400 $km^2$) are more sensitive to climate change than the large catchments, with a large increase in flood volume projections expected.

The present investigation has allowed for an evaluation of the uncertainty level associated with the main elements constituting the ensemble on the flood projections. The results of the variance analysis show that the hydrological models and the climate models are the dominant sources of uncertainty, contributing to 20.9 % and 28.1 % to the total uncertainty (including interactions), respectively. They are followed by the bias correction methods and the RCP scenarios, with the latter playing a minor and almost negligible role in the assessment of climate change impacts on flood projections for the study catchments.

Even though this study was limited by the use of lumped hydrological models, a single objective function and a set of calibration parameters, their inclusion has however contributed to strengthen current practices in the field of hydrological modeling and forecasting of extreme events such as flooding. The careful integration of these, coupled with more realistic flood thresholds, could lead to more relevant results, further pushing the state-of-the-art on the research climate change and flood predictions topic. Nevertheless, this study provides a large-sample overview of an oft-overlooked flooding metric in extreme hydrological climate change impact studies, which can be considered as a starting point for future research regarding the fluvial flood risk assessment.

## CRediT authorship contribution statement

**Alexandre Ionno:** Conceptualization, Methodology, Investigation, Software, Original draft preparation. **Richard Arsenault:** Conceptualization, Draft revision, Supervision, Editing, Funding acquisition. **Magali Troin:** Validation, Writing – original draft, Writing – review & editing. **Jean-Luc Martel:** Investigation, Visualization, Writing – review & editing. **François Brissette:** Investigation, Validation, Writing – review & editing.

## Declaration of competing interest

The authors declare the following financial interests/personal relationships which may be considered as potential competing interests: Richard Arsenault reports financial support was provided by Natural Sciences and Engineering Research Council of Canada.

## Data availability

All data used in this study were taken from the open-access NAC2H database available at http://https://osf.io/s97cd/

## Acknowledgments

This work was supported by the Natural Sciences and Engineering Research Council of Canada (Grant number RGPIN 2018-04872). The authors would like to express their gratitude to the anonymous reviewers who provided insightful comments and suggestions that vastly improved the paper and helped shape it into its current form.

## Appendix A. Supplementary data

Supplementary data to this article can be found online at https://doi.org/10.1016/j.jhydrol.2024.130688.

## References

Aldous, A., Fitzsimons, J., Richter, B., Bach, L., 2011. Droughts, floods and freshwater ecosystems: Evaluating climate change impacts and developing adaptation strategies. Mar. Freshw. Res. 62 (3), 223. https://doi.org/10.1071/MF09285.

Arnell, N.W., Gosling, S.N., 2013. The impacts of climate change on river flow regimes at the global scale. J. Hydrol. 486, 351–364. https://doi.org/10.1016/j.jhydrol.2013.02.010.

Arsenault, R., Brissette, F., Malo, J.-S., Minville, M., Leconte, R., 2013. Structural and Non-Structural Climate Change Adaptation Strategies for the Péribonka Water Resource System. Water Resour. Manag. 27 (7), 2075–2087. https://doi.org/10.1007/s11269-013-0275-6.

Arsenault, R., Brissette, F.P., 2014. Continuous streamflow prediction in ungauged basins: The effects of equifinality and parameter set selection on uncertainty in regionalization approaches. Water Resour. Res. 50 (7), 6135–6153. https://doi.org/10.1002/2013WR014898.

Arsenault, R., Brissette, F., Martel, J.-L., 2018. The hazards of split-sample validation in hydrological model calibration. J. Hydrol. 566, 346–362. https://doi.org/10.1016/j.jhydrol.2018.09.027.

Arsenault, R., Brissette, F., Chen, J., Guo, Q., Dallaire, G., 2020. NAC $^2$ H: The North American Climate Change and Hydroclimatology Data Set. Water Resour. Res. 56 (8) https://doi.org/10.1029/2020WR027097.

Cannon, A.J., 2018. Multivariate quantile mapping bias correction: An N-dimensional probability density function transform for climate model simulations of multiple variables. Clim. Dyn. 50 (1–2), 31–49. https://doi.org/10.1007/s00382-017-3580-6.

Cannon, A.J., Sobie, S.R., Murdock, T.Q., 2015. Bias Correction of GCM Precipitation by Quantile Mapping: How Well Do Methods Preserve Changes in Quantiles and Extremes? J. Clim. 28 (17), 6938–6959. https://doi.org/10.1175/JCLI-D-14-00754.1.

Carvalho-Santos, C., Nunes, J.P., Monteiro, A.T., Hein, L., Honrado, J.P., 2016. Assessing the effects of land cover and future climate conditions on the provision of hydrological services in a medium-sized watershed of Portugal: Impacts of Land Cover and Future Climate on Hydrological Services. Hydrol. Process. 30 (5), 720–738. https://doi.org/10.1002/hyp.10621.

Chen, J., Brissette, F.P., Poulin, A., Leconte, R., 2011. Overall uncertainty study of the hydrological impacts of climate change for a Canadian watershed: Overall Uncertainty Of Climate Change Impacts On Hydrology. Water Resour. Res. 47 (12) https://doi.org/10.1029/2011WR010602.

Chen, J., Brissette, F.P., Chaumont, D., Braun, M., 2013. Finding appropriate bias correction methods in downscaling precipitation for hydrologic impact studies over North America: Evaluation of Bias Correction Methods. Water Resour. Res. 49 (7), 4187–4205. https://doi.org/10.1002/wrcr.20331.

Chen, J., Brissette, F.P., Lucas-Picher, P., 2016. Transferability of optimally-selected climate models in the quantification of climate change impacts on hydrology. Clim. Dyn. 47, 3359–3372.

Cochand, F., Therrien, R., Lemieux, J.-M., 2019. Integrated Hydrological Modeling of Climate Change Impacts in a Snow-Influenced Catchment. Groundwater 57 (1), 3–20. https://doi.org/10.1111/gwat.12848.

Dadhwal, V. K., Aggarwal, S. P., & Mishra, N. (2010). Hydrological simulation of Mahanadi River Basin and impact of LULCC on surface runoff using a macro scale hydrological model.

Dankers, R., Feyen, L., 2008. Climate change impact on flood hazard in Europe: An assessment based on high-resolution climate simulations. J. Geophys. Res. 113 (D19), D19105. https://doi.org/10.1029/2007JD009719.

Devkota, L.P., Gyawali, D.R., 2015. Impacts of climate change on hydrological regime and water resources management of the Koshi River Basin, Nepal. Journal of Hydrology: Regional Studies 4, 502–515. https://doi.org/10.1016/j.ejrh.2015.06.023.

Do, H.X., Westra, S., Leonard, M., 2017. A global-scale investigation of trends in annual maximum streamflow. J. Hydrol. 552, 28–43. https://doi.org/10.1016/j.jhydrol.2017.06.015.

Doll, P., Fiedler, K., & Zhang, J. (2009). Global-scale analysis of river flow alterations due to water withdrawals and reservoirs. Hydrol. Earth Syst. Sci., 20.

Döll, P., Zhang, J., 2010. Impact of climate change on freshwater ecosystems: A global-scale analysis of ecologically relevant river flow alterations. Hydrol. Earth Syst. Sci. 14 (5), 783–799. https://doi.org/10.5194/hess-14-783-2010.

Fluixá-Sanmartín, J., Altarejos-García, L., Morales-Torres, A., Escuder-Bueno, I., 2018. Review article: Climate change impacts on dam safety. Nat. Hazards Earth Syst. Sci. 18 (9), 2471–2488. https://doi.org/10.5194/nhess-18-2471-2018.

Fortin, V., 2000. Le modèle météo-apport HSAMI: historique, théorie et application. Institut de recherche d'Hydro-Québec, Varennes.

Fortin, V., and Turcotte, R. (2007). "Le modèle hydrologique MOHYSE (Bases théoriques et manuel de l'usager).", Département des sciences de la terre et de l'atmosphère, Université du Québec à Montréal, Montréal, 1–17.

Gao, C., Booij, M.J., Xu, Y.-P., 2020. Assessment of extreme flows and uncertainty under climate change: Disentangling the uncertainty contribution of representative

concentration pathways, global climate models and internal climate variability. Hydrol. Earth Syst. Sci. 24 (6), 3251–3269. https://doi.org/10.5194/hess-24-3251-2020.
Giuntoli, I., Villarini, G., Prudhomme, C., Hannah, D.M., 2018. Uncertainties in projected runoff over the conterminous United States. Clim. Change 150 (3–4), 149–162. https://doi.org/10.1007/s10584-018-2280-5.
Guhathakurta, P., Sreejith, O.P., Menon, P.A., 2011. Impact of climate change on extreme rainfall events and flood risk in India. J. Earth Syst. Sci. 120 (3), 359–373. https://doi.org/10.1007/s12040-011-0082-5.
Guo, Q., Chen, J., Zhang, X., Shen, M., Chen, H., Guo, S., 2019. A new two-stage multivariate quantile mapping method for bias correcting climate model outputs. Clim. Dyn. 53 (5), 3603–3623. https://doi.org/10.1007/s00382-019-04729-w.
Gupta, H.V., Kling, H., Yilmaz, K.K., Martinez, G.F., 2009. Decomposition of the mean squared error and NSE performance criteria: Implications for improving hydrological modelling. J. Hydrol. 377 (1–2), 80–91. https://doi.org/10.1016/j.jhydrol.2009.08.003.
Hawkins, E., Sutton, R., 2009. The potential to narrow uncertainty in regional climate predictions. Bull. Am. Meteorol. Soc. 90 (8), 1095–1108.
He, W., Kim, S., Wasko, C., Sharma, A., 2022. A global assessment of change in flood volume with surface air temperature. Adv. Water Resour. 165, 104241 https://doi.org/10.1016/j.advwatres.2022.104241.
Ho, M., Nathan, R., Wasko, C., Vogel, E., Sharma, A., 2022. Projecting changes in flood event runoff coefficients under climate change. J. Hydrol. 615, 128689 https://doi.org/10.1016/j.jhydrol.2022.128689.
Hunter, J., Thyer, M., McInerney, D., Kavetski, D., 2021. Achieving high-quality probabilistic predictions from hydrological models calibrated with a wide range of objective functions. J. Hydrol. 603, 126578 https://doi.org/10.1016/j.jhydrol.2021.126578.
Karmalkar, A.V., Thibeault, J.M., Bryan, A.M., Seth, A., 2019. Identifying credible and diverse GCMs for regional climate change studies—case study: Northeastern United States. Clim. Change 154 (3–4), 367–386. https://doi.org/10.1007/s10584-019-02411-y.
Kim, J., Ivanov, V.Y., Fatichi, S., 2016. Climate change and uncertainty assessment over a hydroclimatic transect of Michigan. Stoch. Env. Res. Risk A 30 (3), 923–944. https://doi.org/10.1007/s00477-015-1097-2.
Knutti, R., Furrer, R., Tebaldi, C., Cermak, J., Meehl, G.A., 2010. Challenges in Combining Projections from Multiple Climate Models. J. Clim. 23 (10), 2739–2758. https://doi.org/10.1175/2009JCLI3361.1.
Koks, E.E., Thissen, M., Alfieri, L., Moel, H.D., Feyen, L., Jongman, B., Aerts, J.C.J.H., 2019. The macroeconomic impacts of future river flooding in Europe. Environ. Res. Lett. 14 (8), 084042 https://doi.org/10.1088/1748-9326/ab3306.
Koneti, S., Sunkara, S., Roy, P., 2018. Hydrological Modeling with Respect to Impact of Land-Use and Land-Cover Change on the Runoff Dynamics in Godavari River Basin Using the HEC-HMS Model. ISPRS Int. J. Geo Inf. 7 (6), 206. https://doi.org/10.3390/ijgi7060206.
Kouchi, D.H., Esmaili, K., Faridhosseini, A., Sanaeinejad, S.H., Khalili, D., Abbaspour, K.C., 2017. Sensitivity of Calibrated Parameters and Water Resource Estimates on Different Objective Functions and Optimization Algorithms. Water 9 (6), 384. https://doi.org/10.3390/w9060384.
Krysanova, V., Donnelly, C., Gelfan, A., Gerten, D., Arheimer, B., Hattermann, F., Kundzewicz, Z.W., 2018. How the performance of hydrological models relates to credibility of projections under climate change. Hydrol. Sci. J. 63 (5), 696–720. https://doi.org/10.1080/02626667.2018.1446214.
Martel, J.-L., Demeester, K., Brissette, F. O., Poulin, A., & Arsenault, R. 2017. HMETS—A Simple and Efficient Hydrology Model for Teaching Hydrological Modelling, Flow Forecasting and Climate Change Impacts. 11.
Masson-Delmotte, V., Zhai, P., Pirani, A., Connors, S. L., Péan, C., Berger, S., … Zhou, B. (Eds.). (2021). Summary for policymakers. In Climate Change 2021: The Physical Science Basis. Contribution of Working Group I to the Sixth Assessment Report of the Intergovernmental Panel on Climate Change (pp. 3–32). Cambridge, United Kingdom and New York, NY, USA: Cambridge University Press. doi: 10.1017/9781009157896.001.
Maurer, E.P., Brekke, L.D., Pruitt, T., 2010. Contrasting Lumped and Distributed Hydrology Models for Estimating Climate Change Impacts on California Watersheds1: Contrasting Lumped and Distributed Hydrology Models for Estimating Climate Change Impacts on California Watersheds. JAWRA Journal of the American Water Resources Association 46 (5), 1024–1035. https://doi.org/10.1111/j.1752-1688.2010.00473.x.
Miller, S.N., Kepner, W.G., Mehaffey, M.H., Hernandez, M., Miller, R.C., Goodrich, D.C., Miller, W.P., 2002. Integrating Landscape Assessment And Hydrologic Modeling For Land Cover Change Analysis. J. Am. Water Resour. Assoc. 38 (4), 915–929. https://doi.org/10.1111/j.1752-1688.2002.tb05534.x.
Mittal, N., Bhave, A.G., Mishra, A., Singh, R., 2016. Impact of Human Intervention and Climate Change on Natural Flow Regime. Water Resour. Manag. 30 (2), 685–699. https://doi.org/10.1007/s11269-015-1185-6.
Mohammed, I.N., Bomblies, A., Wemple, B.C., 2015. The use of CMIP5 data to simulate climate change impacts on flow regime within the Lake Champlain Basin. J. Hydrol. Reg. Stud. 3, 160–186.
Murdoch, P.S., Baron, J.S., Miller, T.L., 2000. Potential Effects Of Climate Change On Surface-Water Quality In North America [1]. JAWRA Journal of the American Water Resources Association 36 (2), 347–366. https://doi.org/10.1111/j.1752-1688.2000.tb04273.x.
Muzik, I., 2002. A first-order analysis of the climate change effect on flood frequencies in a subalpine watershed by means of a hydrological rainfall–runoff model. J. Hydrol. 267 (1–2), 65–73. https://doi.org/10.1016/S0022-1694(02)00140-3.
Nash, J.E., Sutcliffe, J.V., 1970. River flow forecasting through conceptual models part I — A discussion of principles. J. Hydrol. 10 (3), 282–290. https://doi.org/10.1016/0022-1694(70)90255-6.
Obeysekera, J., Irizarry, M., Park, J., Barnes, J., Dessalegne, T., 2011. Climate change and its implications for water resources management in south Florida. Stoch. Env. Res. Risk A 25 (4), 495–516. https://doi.org/10.1007/s00477-010-0418-8.
Paul, M., Negahban-Azar, M., 2018. Sensitivity and uncertainty analysis for streamflow prediction using multiple optimization algorithms and objective functions: San Joaquin Watershed, California. Modeling Earth Systems and Environment 4 (4), 1509–1525. https://doi.org/10.1007/s40808-018-0483-4.
Perrin, C., Michel, C., Andréassian, V., 2003. Improvement of a parsimonious model for streamflow simulation. J. Hydrol. 279 (1–4), 275–289. https://doi.org/10.1016/S0022-1694(03)00225-7.
Poulin, A., Brissette, F., Leconte, R., Arsenault, R., Malo, J.-S., 2011. Uncertainty of hydrological modelling in climate change impact studies in a Canadian, snow-dominated river basin. J. Hydrol. 409 (3–4), 626–636. https://doi.org/10.1016/j.jhydrol.2011.08.057.
Prudhomme, C., Jakob, D., Svensson, C., 2003. Uncertainty and climate change impact on the flood regime of small UK catchments. J. Hydrol. 277 (1), 1–23. https://doi.org/10.1016/S0022-1694(03)00065-9.
Rasouli, K., Pomeroy, J.W., Whitfield, P.H., 2019. Are the effects of vegetation and soil changes as important as climate change impacts on hydrological processes? Hydrol. Earth Syst. Sci. 23 (12), 4933–4954. https://doi.org/10.5194/hess-23-4933-2019.
Schnorbus, M., Werner, A., Bennett, K., 2014. Impacts of climate change in three hydrologic regimes in British Columbia, Canada: Impacts Of Climate Change In British Columbia. Hydrol. Process. 28 (3), 1170–1189. https://doi.org/10.1002/hyp.9661.
Sun, X., Li, R., Shan, X., Xu, H., Wang, J., 2021. Assessment of climate change impacts and urban flood management schemes in central Shanghai. Int. J. Disaster Risk Reduct. 65, 102563 https://doi.org/10.1016/j.ijdrr.2021.102563.
Sunyer, M.A., Hundecha, Y., Lawrence, D., Madsen, H., Willems, P., Martinkova, M., Yücel, I., 2015. Inter-comparison of statistical downscaling methods for projection of extreme precipitation in Europe. Hydrol. Earth Syst. Sci. 19 (4), 1827–1847. https://doi.org/10.5194/hess-19-1827-2015.
Tabari, H., 2020. Climate change impact on flood and extreme precipitation increases with water availability. Sci. Rep. 10 (1), 13768. https://doi.org/10.1038/s41598-020-70816-2.
Taylor, K.E., Stouffer, R.J., Meehl, G.A., 2012. An Overview of CMIP5 and the Experiment Design. Bull. Am. Meteorol. Soc. 93 (4), 485–498. https://doi.org/10.1175/BAMS-D-11-00094.1.
Troin, M., Caya, D., Velázquez, J.A., Brissette, F., 2015. Hydrological response to dynamical downscaling of climate model outputs: A case study for western and eastern snowmelt-dominated Canada catchments. J. Hydrol.: Reg. Stud. 4, 595–610. https://doi.org/10.1016/j.ejrh.2015.09.003.
Troin, M., Arsenault, R., Martel, J.-L., Brissette, F., 2018. Uncertainty of Hydrological Model Components in Climate Change Studies over Two Nordic Quebec Catchments. J. Hydrometeorol. 19 (1), 27–46. https://doi.org/10.1175/JHM-D-17-0002.1.
Valéry, A., Andréassian, V., Perrin, C., 2014. 'As simple as possible but not simpler': What is useful in a temperature-based snow-accounting routine? Part 2–Sensitivity analysis of the Cemaneige snow accounting routine on 380 catchments. J. Hydrol. 517, 1176–1187.
van Vliet, M.T.H., Franssen, W.H.P., Yearsley, J.R., Ludwig, F., Haddeland, I., Lettenmaier, D.P., Kabat, P., 2013. Global river discharge and water temperature under climate change. Glob. Environ. Chang. 23 (2), 450–464. https://doi.org/10.1016/j.gloenvcha.2012.11.002.
Veijalainen, N., Lotsari, E., Alho, P., Vehviläinen, B., Käyhkö, J., 2010. National scale assessment of climate change impacts on flooding in Finland. J. Hydrol. 391 (3–4), 333–350. https://doi.org/10.1016/j.jhydrol.2010.07.035.
Wang, H., Chen, J., Xu, C., Zhang, J., Chen, H., 2020. A Framework to Quantify the Uncertainty Contribution of GCMs Over Multiple Sources in Hydrological Impacts of Climate Change. Earth's Future 8 (8). https://doi.org/10.1029/2020EF001602.
Wilby, R.L., Harris, I., 2006. A framework for assessing uncertainties in climate change impacts: Low-flow scenarios for the River Thames, UK. Water Resour. Res. 42 (2) https://doi.org/10.1029/2005WR004065.
Zhou, Q., Leng, G., Su, J., Ren, Y., 2019. Comparison of urbanization and climate change impacts on urban flood volumes: Importance of urban planning and drainage adaptation. Sci. Total Environ. 658, 24–33. https://doi.org/10.1016/j.scitotenv.2018.12.184.